

BrainNet-7: A CNN Model for Diagnosing Brain Tumors from MRI Images based on an Ablation Study

Md Harun or Rashid, Salma Akter, Amatul Bushra Akhi
Dept. of Computer Science Engineering
Daffodil International University
Dhaka, Bangladesh

Abstract—Tumors in the brain are masses or clusters of abnormal cells that may spread to other tissues nearby and pose a danger to the patient. The main imaging technique used to determine the extent of brain tumors is magnetic resonance imaging, which ensures an accurate diagnosis. A sizable amount of data for model training and advances in model designs that provide better approximations in a supervised environment likely account for most of the growth in Deep Learning techniques for computer vision applications. Deep learning approaches have shown promising results for increasing the precision of brain tumor identification and classification using magnetic resonance imaging (MRI). This study's purpose is to describe a robust deep-learning model that categorizes brain tumors using MRI images into four classes based on a convolutional neural network (CNN). By removing artefacts, reducing noise, and enhancing the image, unwanted areas of brain tumors are deleted, quality is improved, and the tumor is highlighted. Several CNN architectures, including VGG16, VGG19, MobileNet, MobileNetV2, and InceptionV3, are investigated to compare or get the best model. After getting the best model, a hyper parameter ablation study was performed on that model. Proposed BrainNet-7 achieved the best results with 99.01% test accuracy and 99.21% test and validation accuracy.

Keywords—MRI image; image pre-processing; transfer-learning; CNN; brainnet-7

I. INTRODUCTION

A brain tumor is one of the tenth most common causes of mortality in men and women regarding the brain or central nervous system, often referred to as the CNS [1]. It is estimated that 40% of all cancer types develop brain cancer as a result of metastasis rather than death from brain tumors [2]. In 2000, June 8 was designated World Brain Tumor Day to raise understanding and educate people regarding brain tumors [3]. If abnormal cells begin to grow unnecessarily in the brain or spinal cord, it is known as a brain tumor. The World Health Organization categorized brain tumors into four groups on the basis of molecular characteristics in 2016 -- I, II, III, and IV [3, 4]. Brain tumor patients have a very low life probability when the tumor is in more advanced phase [5]. Therefore, accurate and timely cancer diagnosis and grade estimation

enhance illness prognosis and treatment options. A neurological examination, imaging, biopsies, and other methods are used to determine the grade and diagnosis of tumors [3, 6]. Doctors use magnetic resonance imaging (MRI) before and after treatment to determine the tumor's shape. As a result, surgical resections can be planned and monitored as the illness develops [7]. Early classification of brain tumor grade plays an important role in successful prognosis [8]. A good contrast enhancement and noninvasive MRI images make it the preferred imaging technique in glioma diagnosis [9]. Radiologists observe and diagnose tumors using the conventional method, it is laborious and time-consuming. Computer-aided medical diagnosis (CAMD) has made great strides with artificial intelligence (AI) and deep learning, which can assist doctors in interpreting medical images within seconds [10]. A dataset's quality and size significantly impact the performance of deep learning technology. Images with high-quality annotations are required for deep learning techniques. However, labelling large quantities of medical images is quite challenging since annotation is a time- and expertise-intensive process [11]. Two significant barriers to deep learning in medical imaging are insufficient imaging data and a lack of annotations from human experts [11]. The above challenges have been addressed and resolved through numerous efforts. A transfer learning strategy can be helpful when there are only a few domain samples for training. Typically, it refined on the architecture that has already pre-trained on a largest, labelled dataset. The transfer of learning knowledge to the target dataset makes network convergence speed faster while maintaining low computational complexity [12].

In this work, we propose a CNN model BrainNet-7, which is fine-tuned network and classifies brain tumor MRI images most correctly. Firstly, use, five pre-trained models, VGG16, VGG19, MobileNet, MobileNetV2, and InceptionV3, are employed in the dataset and then use proposed a CNN model. After in the CNN model a hyper parameter ablation was performed for getting the robust and fine-tuned model. This model is given the best accuracy among all the previous networks (see Fig. 1).

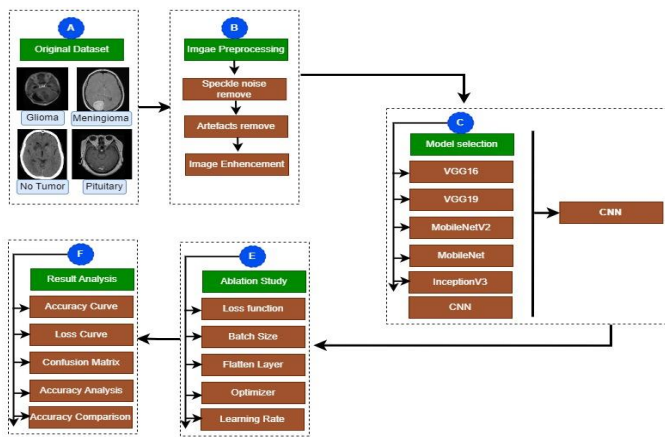


Fig. 1. An overview of the entire classification process.

II. LITERATURE REVIEW

A classification approach was provided by Santhosh and his colleagues to distinguish between normal and abnormal brain tissues. The segmentation of the system was based on threshold and watershed. SVM provided overall classification accuracy of 85.32 percent [13].

Arunkumar and his research associates created a world-class brain tumor classification architecture on the basis on traditional machine vision techniques like Fourier transform image enhancement, completely automated trainable segmentation, histogram-of-oriented-gradients (HOG) feature extraction, and an ANN-based classification model. Size, circularity, and gray-scale average are used to filter out non-ROI brain components and a k-fold-cross validation technique, the constructed model successfully distinguished between normal and pathological brain slices with the accuracy of 92.14%. [14].

A brain tumor categorization algorithm based on brain MRIs obtained from RD-BVH was proposed by Hafeez Ullah and research fellows. Brain MRI slices' intensity, shape, and texture features were retrieved, and the proposed methodology achieved 97% accuracy [15].

An approach for classifying tumors that uses CNN and a genetic algorithm was proposed by Amin Kabir et al. in 2019 [16]. To reduce validation error, the authors used a genetic algorithm. Prior to the CNN architecture, the images were rescaled using data normalization, and they underwent augmentation to achieve perfect rotation. The accuracy was 94.2% using the recommended procedure. The new method, according to the authors, is sufficiently successful to detect tumors.

Biswas et al. in 2021[17] an efficient training feature. The proposed network construction method, known as "Levenberg-Marquardt," offers 95.4% accuracy, 94.58% sensitivity, and 97.83% specificity. Comparatively speaking, this improved result outperforms other current detection methods. Getting great results comes down to two main things: using the right preprocessing steps and a powerful training function.

Brain cancers can be identified and classified from MRI images using a quicker Region-based CNN (faster R-CNN) technique used by Avşar, E. et al. [18]. Their model's accuracy was 91.66% as measured. In study [19], a method for classifying MRI brain cancer was also suggested that uses SVM with grayscale, symmetry, and texture features to get information about features.

Precious et al. [20] propose three optimizers, including ADAM, SGDM, and RMSprop, from whom detection accuracy of 98.1%, 92.5%, and 83.0% is attained. In order to detect tumors, four supervised machine learning classifiers are used once the features have been retrieved using CNN. Discriminant analysis, Naive Bayes, SVM, and KNN classifiers are among the classifiers that are employed. 96.2%, 94.3%, 75.0%, and 96.2% of the classifiers' accuracy were obtained, respectively.

Papageorgiou et al. [21] created the fuzzy cognitive map (FCM) approach to represent model experts. A computationally sophisticated training technique known as the activation Hebbian algorithm was added to the FCM ranking model to enhance its classification capabilities. Medical resources, which included 100 instances, were used to verify the proposed method. For low-grade and high-grade brain tumors, the FCM model correctly diagnosed patients in 90.26% (37/41) and 99.22% (55/59) of the cases, respectively. Comparing the proposed model's results to those of current algorithms like fuzzy decision trees and decision trees, the proposed model's results show a marginally higher accuracy. The same kind of first-hand data was used to compare them, and while they were able to get high accuracy, they couldn't get high memory.

In order to work with 2D (two-dimensional) images, John Schmeelk [22] used a two-dimensional wavelet transform (2D-WT). The comparison of the two transforms on separated elements was covered in depth by the authors. A similar image was also subjected to a comparison of the global qualities offered by the Fourier transform (FT) approach and the wavelet transform. The Gaussian subfield wavelet was chosen for this study because, for some reason, it made it possible to compare it to the Fourier technique.

In our findings we are improving the model and get the high accuracy from the model. In our approach firstly we decrease noise by using various image processing techniques and then we are developed a model which give us the best accuracy and our approach beat all the existing model.

III. DATASET DESCRIPTION

The Brain Tumor MRI dataset has a total of 7022 MRI images analyzed for this research. There are four classes in the dataset: glioma, meningioma, no tumor, and pituitary. There are 1621 images in the glioma class, 1645 images in the meningioma class, 2000 images in the no tumor class, and 1757 images in the pituitary class. All images of this datasets are 512×512 pixels in grayscale presentation. The dataset was taken from the open-source website Kaggle. As shown in Table I, Fig. 2 the dataset is described in detail:

TABLE I. SHOW THE DATASET DESCRIPTION

Name	Description
Total Number of Images	7022
Average Dimension	512 x 512
Color Grading	Grayscale
Data Format	JPG
Glioma	1621
Meningioma	1645
No Tumor	2000
Pituitary	1757

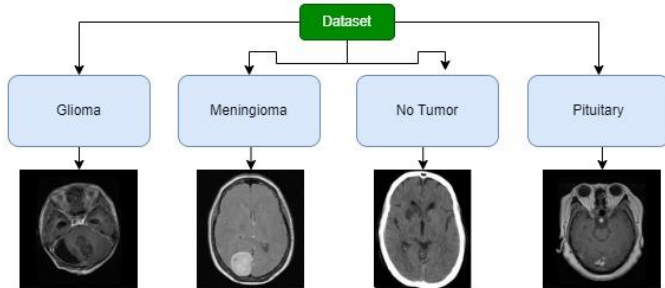


Fig. 2. Brain Tumor MRI dataset containing four classes with various noise and artifacts.

A. Image Processing

There is a lot of noise and artefacts in brain tumor MRI dataset images, so this study focuses on improving the model's accuracy through image processing techniques. Because images are usually filled with noise and artefacts, image processing is the first step in training a deep-learning model. First, a median filter is used to remove noise from this image, then a morphological opening is used to remove artefacts.

B. Remove Spackle Noise

The brain tumour MRI dataset has spackle noise, as previously stated. Median filters are useful for removing spackle noise.

C. Median Filter

Median filter is a well-known order-statistic filter that excels at removing certain types of noise, including Gaussian, random, and salt-and-pepper noise. The image of this step is given in Fig. 3.

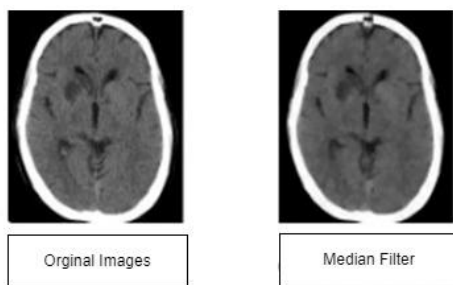


Fig. 3. Median filtered images.

The first photo are the original images and the second photo is the output of the median filter.

D. Artifact Removal

In addition to the brain tumour MRI dataset having artefacts, morphological operations are used to remove these artefacts [23]. Various morphological operations can be used for eliminating artifacts, but this study uses morphological opening techniques.

E. Morphological Opening

The kernel size of the filter depends on the operation to be performed. The output of this step is shown in Fig. 4.

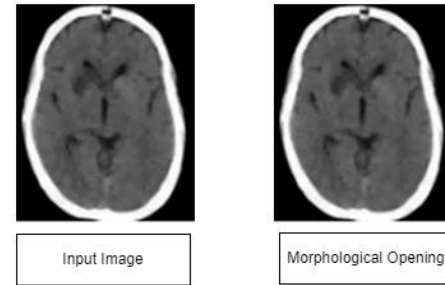


Fig. 4. Output of the morphological opening.

The first image are the input images which we get from the median filter and the second photo is the output of the morphological opening.

$$g(j, s) = f(j, s) * u(j, s) + (j, s) \quad (1)$$

Where,

$g(j,s)$ – debase image $u(j,s)$ – multiplicative noise

$f(j,s)$ – original image $\eta(j,s)$ – additive noise

Before diagnosis, removing additive noise from ultrasound images is necessary, but multiplicative noise can be allowed, given in the equation below:

$$g(j, s) = f(j, s) * u(j, s) + \eta(j, s) - \eta(j, s) \quad (2)$$

$$g(j, s) = f(j, s) * u(j, s) \quad (3)$$

F. Clahe

The Clahe technique is used to balance the overall contrast. A further sophisticated version of adaptive histogram equalization is called CLAHE. Clahe was developed to improve the quality of medical imaging of complex structures [24, 25]. The output of this step is shown in Fig. 5.

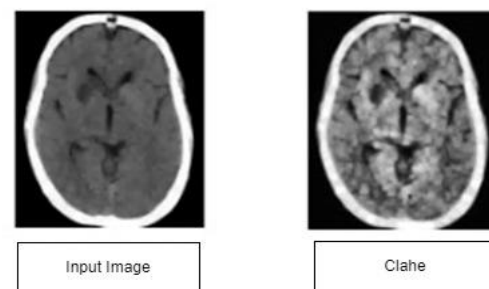


Fig. 5. Output of the clahe.

The first images are the original images and the second images are the output of the CLAHE.

Let an image size be $M \times M$ and each tile size for image is $m \times m$ then the total number of tiles is calculating as:

$$T = \frac{M \times M}{m \times m} \quad (3)$$

Clip limit $C_L = M_{CL} \times M_{avg}$ is used to construct the histograms for these tiles.

Where,

M_{CL} = normalized contrast limit. M_{AVG} = total pixels average value.

The equation of pixels average is (3):

$$M_{AVG} = \frac{M \times M \times My}{Mg} \quad (4)$$

Where,

Mg = total gray levels Mx and My = total pixels of x and y dimension

$$M_{CP} = \frac{M \sum cl}{Mg} \quad (5)$$

Where,

C_L = the clipped pixel.

$$M_r = \frac{Mg}{M_r} \quad (6)$$

Where,

M_r is remaining number of clipped pixels

clahe formula:

$$I_c(p, q) = T(t(p, q) = \frac{(L-1)}{PQ} \sum_j^K n_j \quad (7)$$

G. Verification

It is possible to lose a lot of image quality when using many image preprocessing algorithms, so various types of geometric analysis like PSNR, SSIM, MSE, and RMSE are performed to determine if the image quality has been compromised.

H. MSE

MSE describes the pixels of the two pictures under comparison as having a cumulative squared error. A value close to 0 indicates acceptable image quality, while the MSE value ranges from 0 to 1. A value of 0 indicates a picture with no noise. Values higher than 0.5 indicate a decline in quality.

$$MSE = \frac{1}{AB} \sum_{i=0}^{r-1} \sum_{j=0}^{n-1} (O(r, s) - P(r, s))^2 \quad (8)$$

Where,

The ground truth image is O , the image which is processed is P and A, B denote the pixels of O and P , and r, s denote pixel rows of p, q .

I. PSNR

Calculating PSNR begins with calculating MSE. PSNR is then estimated using the following formula:

$$PSNR = 10 \log_{10} \left(\frac{Q^2}{MSE} \right) \quad (9)$$

Q is the highest fluctuation in the input image data type. A maximum of 255 pixels is used as image maximum value. Typically, PSNR should be between 30 and 50 dB for an 8-bit image [26].

J. SSIM

SSIM measures the decline in image condition caused by preprocessing processes. In this estimation, 1 indicates "perfect structural similarity" and 0 means "no structural similarity" [9].

$$SSIM(r, s) = \frac{(2\mu_x\mu_y + c_1)(2\sigma_{xy} + c_2)}{(\mu_x^2 + \mu_y^2 + c_1)(\sigma_x^2 + \sigma_y^2 + c_2)} \quad (10)$$

Where,

r, s is two image, σ_r^2, σ_s^2 is variance, σ_{rs} is covariance of the images and μ_r, μ_s is the average of two image calculated using the Gaussian window.

K. RMSE

Image quality is measured by RMSE, which compares the original and processed images. RMSE values near 0 indicate good image quality and fewer errors.

$$RMSE = \sqrt{\sum_{j=1}^N (d_{fi} - \frac{d_d}{N})^2} \quad (11)$$

Where, d_{fi} is the different of predict value, d_d is the actual value, N is the Size of the Dataset.

TABLE II. SHOWN PSNR, MSE, SSIM, RMSE

Image	MSE	PSNR	SSIM	RMSE	Image
Image_1	15.17	39.35	0.962	0.13	Image_1
Image_2	13.63	40.66	0.961	0.13	Image_2
Image_3	14.25	42.59	0.964	0.11	Image_3
Image_4	13.13	38.28	0.968	0.12	Image_4
Image_5	12.38	45.47	0.962	0.09	Image_5

In this Table II we are showing some statistical value which proved that our image processing techniques are the best. Image quality is not damaged after image preprocessing.

IV. DATA SPLIT

After analyzing the statistical value of the image, the full dataset is divided into three segments (training set, validation set, and testing set). Three splitting ratios for training-testing data (90:10, 80:20, and 70:30) are often used to evaluate the effect of the overall accuracy of a model is affected by the size of the training-testing data [27]. According to this study, the 70:30 ratio means 70% train sets, 10% validation sets, and 20% test sets.

V. PROPOSED MODEL

As previously said, this research explored with a total of five transfer learning network to identify the ideal network based on accuracy in order to discover the best transfer learning model for the classification issue. Transfer Learning

Model: There are five pre-trained models total—InceptionV3, MobileNetV2, MobileNet VGG16, and VGG19—that are trained on training data and tested on testing data.

A. VGG-16

Simonyan and Zisserman [28] introduced the DCNN model known as VGG16. The model achieving 92.7% top 5 test accuracy in the ImageNet dataset [29]. A VGG16 produced a substantially greater accuracy than a fully trained architecture, according to studies on the efficiency of transfer learning [30]. The kernel may learn more complicated characteristics with the help of the VGG model's enhanced depth. The VGG16 architecture is a convolutional neural network set. It is regarded as one of the best computer vision models to date. VGG16 is unusual in that it only employs 3 x 3 filter convolution layers with a stride 1 and always uses the same padding and maxpool layer with a 2 x 2 filter stride 2. VGG16 has 16 layers. Spatial pooling is achieved in this model by employing five max pooling layers. After a sequence of convolutional layers, three fully connected (FC) layers are added. Finally, there's the softmax layer. In all networks, always set the layers 1 and 2 in the same way.

B. VGG-19

There are 19 layers in the VGG19 model, a variation of the VGG model. The VGG19 model concludes with three additional FC layers, totaling 19 layers with 4096, 4096, and 1000 neurons in each layer. Moreover, five Maxpool layers are included as well as a Softmax layer. It is a characteristic of convolutional layers that ReLU is activated. Non-linearity is included into models using Rectified linear units (ReLU), which increases classification and compute performance. Three layers were built, all of which were entirely interconnected. Finally, there is a softmax function as the model's final layer.

C. MobileNet

The MobileNet model is TensorFlow's first computer vision model designed specifically for mobile applications. MobileNet employs depth-wise separable convolutions. The number of parameters is dramatically reduced compared to a network with regular convolutions of the same depth. As a result, portable deep neural networks have been developed. To generate a depth-separable convolution, two techniques are used.

- In-depth convolution.
- Convolution at the point of interest.

MobileNet, a CNN class that Google freely licenses, is a great starting point for training our ultra-short and ultra-fast classifiers.

D. MobileNetV2

The Google community has suggested MobileNetV2. There are two kinds of blocks in it, and each block has three levels. Each block has 11 convolutional layers with 32 filters in the first, third, and second layers. All layers use the rectified linear activation function (ReLU). In order to prevent non-linearity from corrupting a significant volume of data, longitudinal bottlenecks are essential between layers. There is

a difference between the strides of the two blocks, with block 1 having a stride of one and block 2 having a stride of two.

E. InceptionV3

A new InceptionV3 design aims to reduce the needed computational power by modifying earlier Inception designs. It is possible to decrease the computational cost by regularizing, reducing the dimension, factorizing convolutions, and parallelizing computations.

F. BrainNet-7

The BrainNet-7 has three convolutional layers and one max pool layer for each convolutional layer Fig. 6. There are 3 X 3 convolutional kernels in the model. There is a dropout value of 0.5 in the first block of the convolutional kernel, and 32 in the second block of the convolutional kernel. 'Relu' has been selected as the activation function for the final layer, followed by 'SoftMax'. Using batch size 32 and Adam optimizer, categorical crossentropy was used as a loss function. There is an 0.001 learning rate.

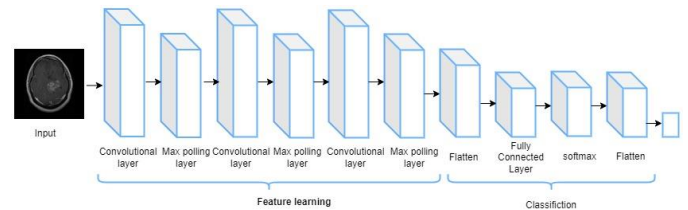


Fig. 6. BrainNet-7 model architecture.

VI. TRAINING APPROACH

For training the models, the batch size is 16, and the maximum number of epochs is 100[31]. During training, Keras' "callback" function was used to store the weights of the best model based on a minimal loss value [32]. Adam has been used as an optimizer at a learning rate of 0.001. Categorical cross-entropy is the defaulting loss function for multiclass challenges [33]. In order to forecast the probability for each class, 'Softmax' activation is used. Since Softmax normalizes all values between 0 and 1, their aggregate always equals 1.

$$\text{Softmax}(y_i) = \frac{\exp(y_i)}{\sum_j \exp(y_j)} \quad (12)$$

VII. ABLATION STUDY

An ablation study is often carried out in CNN-based applications to evaluate the model's stability and performance after deleting or changing various layers and hyperparameters. Using hyperparameter ablation to develop a robust and fine-tuned network in this study.

VIII. RESULT AND DISCUSSION

In this section, several performance matrix are shown as mathematically.

$$\text{ACC} = \frac{TP+TN}{TP+TN+FP+FN} \quad (13)$$

$$\text{Recall} = \frac{TP}{TP+FN} \quad (14)$$

$$\text{Specificity} = \frac{TN}{TN+FP} \quad (15)$$

$$\text{Precision} = \frac{TP}{TP+FP} \quad (16)$$

$$\text{ACC} = 2 \frac{\text{precision} * \text{recall}}{\text{precision} + \text{recall}} \quad (17)$$

$$\text{FPR} = \frac{FP}{FP+TN} \quad (18)$$

A. Result of Transfer Learning and CNN Model

Table III shows the training accuracy, test accuracy, validation accuracy, and train, test and validation loss for the five transfer learning models. The CNN model has the highest accuracy, as can be seen in the table.

TABLE III. RESULT OF TRANSFER LEARNING AND CNN MODEL

Model	Train_Accuracy	Train_Loss	Val_Accuracy	Val_Loss	Test_Accuracy
VGG19	96.67	0.22	95.63	0.21	95.24
VGG16	97.77	0.18	96.83	0.12	96.13
Mobile Net	95.43	0.18	94.23	0.28	94.24
Mobile Net V2	95.76	0.25	94.63	0.32	94.59
InceptionV3	76.86	0.421	76.21	0.392	76.21
CNN	97.91	0.15	97.95	0.11	97.95

In this table we are showing the Accuracy of the all model which we employing in this study.

IX. RESULT AND ABLATION STUDY

It is possible to improve classification accuracy by changing several design components to make it more reliable. A total of five studies are run as an ablation study, modifying various BrainNet-7 elements based on the optimized VGG16 architecture.

A. Case Study-1 Changing Flatten Layer

In case study 1, it is shown in Table IV that the flatten layer provides the highest accuracy when it is used. Additionally, global average and global maximum pooling do not provide good accuracy. Flattening the layer gives 96.93% accuracy, while global max and global average pooling give 95.24 and 96.83% accuracy, respectively.

TABLE IV. CHANGING FLATTEN LAYER

Configuration No.	Flatten layer type	Epoch x training time	Test accuracy (%)	Finding
1	Flatten	97 x 5s	97.95%	Highest accuracy
2	Global Max pooling	60 x 4s	95.24%	Accuracy dropped
3	Global Average pooling	54 x 5s	96.83%	Accuracy dropped

B. Case Study-2 Changing the Batch Size

Changing the batch size is the subject of case study two. A batch size of 32 is the most accurate, followed by 32, 64, and 16. When the batch size is 32 the test accuracy is 96.39%.

C. Case Study-3 Changing Loss Function

Case study 3 experiments with changing loss functions and finds that categorical cross-entropy gives the best outcomes, (Table V) 96.93%.

TABLE V. CHANGING LOSS FUNCTION

Configuration No.	Loss Function	Epoch x training time	Test accuracy (%)	Finding
1	Binary Crossentropy	Error	Error	Error
2	Categorical Crossentropy	43 x 5s	98.13%	Highest accuracy
3	Mean Squared Error	96 x 5s	96.82%	Accuracy dropped
4	Mean absolute error	12 x 4s	68.25%	Accuracy dropped
5	Mean squared logarithmic error	45 x 5s	96.83%	Accuracy dropped

D. Case Study-4 Changing Optimizer

Adam optimizer provides the highest accuracy when compared to Nadam, SGD, and ADamax optimizers in case study 4 (Table VI).

TABLE VI. CHANGING LOSS OPTIMIZER

Configuration No.	Optimizer	Epoch x training time	Test accuracy (%)	Finding
1	Adam	97 x 5s	98.41%	Highest accuracy
2	Nadam	44 x 5s	98.13%	Previous dropped
3	SGD	90 x 5s	84.13%	Accuracy dropped
4	Adamax	88 x 5s	90.48%	Accuracy dropped

E. Case Study-5 Changing Learning Rate

In comparison to 0.001, 0.0001, and 0.01, when using 0.01 provide the highest accuracy (Table VII).

TABLE VII. CHANGING LEARNING RATES

Configuration No.	Learning rate	Epoch x training time	Test accuracy (%)	Finding
1	0.01	92 x 55s	98.41	Accuracy dropped
2	0.001	97 x 5s	98.43%	Highest accuracy
3	0.0001	68 x 57s	97.28	Accuracy improved

F. Performance Analysis of Best Model

After executing the ablation study on the suggested BrainNet-7 model, an improvement in classification accuracy is shown on CNN model. A summary of BrainNet-7 final setup is provided in Table VIII.

TABLE VIII. EVALUATED PERFORMANCE OF BEST MODEL

Table with 2 columns: Configuration, Value. Rows include Size of images (224 x 224), Epoch (97), Optimizer (Adam), Learning rates (0.001), Batch sizes (16), Activation functions (Softmax), Dropouts (0.5), Momentums (0.9), Accuracy (98.43).

G. Performance Analysis and Statistical Analysis

In Table IX show the FPR, FNR, FDR, KC, MCC, MAE and RMSE of the best hyper-tuned CNN (BrainNet-7) model.

TABLE IX. PERFORMANCE ANALYSIS AND STATISTICAL ANALYSIS

Table with 8 columns: Accuracy, FPR (%), FNR (%), FDR (%), KC (%), MCC (%), MAE, RMSE. Row 1: 98.43, 1.46, 2.22, 2.59, 99.01, 88.35, 2.09, 5.79.

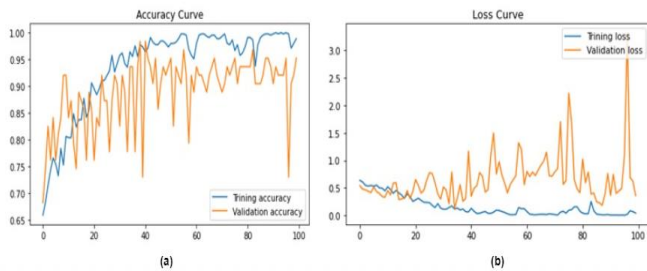


Fig. 7. Losses and accuracy curve.

Fig. 7 shows the accuracy and loss curves for the best-performing model. The training curve converges without bumps from the first to the final epoch. Based on the difference between validation and training accuracy curves, there is no evidence of overfitting in the course of training. As with the training curve, the loss curve in figures 6 unites smoothly to the end epoch. The trainings and losses curves indicate that neither overfitting nor underfitting occurred. The confusion matrix is also shown in Fig. 7.

H. Comparison with Existing Work

This section Table X compares the proposed CNN models (BrainNet-7) to classify. The accuracy, reliability and competency of these earlier investigations and our suggested methods are compared in Table VIII.

TABLE X. COMPARISON BETWEEN PROPOSEDMODEL AND PREVIOUS STUDY

Table with 4 columns: Paper, Dataset, Classifier, Accuracy. Rows include [13] (MRI, SVM, 85.23%), [14] (MRI, ANN, 92.14%), [15] (MRI, Machine Learning Classifier, 97.00%), [16] (MRI, CNN, 94.2%), [17] (MRI, CNN, 95.4%), [18] (MRI, Faster-R-CNN, 91.66%), [20] (MRI, Machine learning classifier, 98.1%), Proposed Model (BrainNet-7) (MRI, Fine-tuned Transfer Learning, 98.43).

X. CONCLUSION

For training, deep learning systems for tumor identification in medical imaging need massive, annotated datasets. Subspecialty, radiologists often manually annotate images. AI's progress in medical imaging is hampered by unreasonably high related costs (time and expertise). Transfer learning techniques have been studied to train a competitive classifier with the least amount of annotation expense. Transfer learning is a popular technique that allows models to apply the information they have gained on massive datasets to new recognition and classification tasks. This study proposes a system based on a transfer learning model for classifying brain tumor MRI images more accurately which can reduce the death ratio. This experiment uses various preprocessing techniques to remove speckle noise and artefacts from the image. Five transfer learning models have been experimented with in the Brain Tumor MRI dataset. After that, a hyperparameter ablation study is conducted on the best-performed transfer learning model to get the best outcome from the model. The proposed model has been fine-tuned with proper hyperparameters, that's why it gained the highest accuracy.

XI. LIMITATIONS AND FUTURE SCOPE

The suggested CNN models for multiclass classification outperformed traditional classifiers considerably, according to the whole discourse of this work. The dataset for the suggested model is too small—it only contains 7022 images—and the study's major limitation—the leakage of a significant amount of genuine medical data—can be solved in the future. As a result, it is possible to expand the quantity of unprocessed medical photos and assess the performance of the suggested model using real-time medical data in the future. The suggested model of this research does, however, successfully categorize the four types of brain tumor classes in the majority of test instances. It is feasible to make sure that the recommended fine-tuned CNN model is accurate and improved in all areas of diagnosis, despite a few small disadvantages.

REFERENCES

- [1] Cancer statistics [Online]. Available: <https://www.cancer.net/cancer-types/bra-in-tumor/statistics>. Accessed: 17-Feb-2020.
- [2] Cancer statistics [Online]. Available: https://www.nhp.gov.in/world-brain-tumour-day2019_pg, 2019. Accessed: 17-Feb-2020.
- [3] G.S. Tandel, M. Biswas, O.G. Kakde, A. Tiwari, H.S. Suri, M. Turk, B. K. Madhusudhan, L. Saba, J.S. Suri, A review on a deep learning perspective in brain cancer classification, *Cancers* 11 (1) (2019) 111, <https://doi.org/10.3390/cancers11010111>.
- [4] D.N. Louis, A. Perry, G. Reifenberger, D.A. von, D. Figarella-Branger, W. K. Cavenee, H. Ohgaki, O.D. Wiestler, P. Kleihues, Ellison DW the 2016 World G.S. Tandel et al. *Computers in Biology and Medicine* 122 (2020) 103804 28 Health Organization classification of tumors of the central nervous system: a summary, *Acta Neuropathol.* 131 (2016) 803–820, <https://doi.org/10.1007/s00401-016-1545-1>.
- [5] S. Pereira, A. Pinto, V. Alves, C.A. Silva, Brain tumor segmentation using convolutional neural networks in MRI images, *IEEE Trans. Med. Imag.* 35 (5) (2016) 1240–1251, <https://doi.org/10.1109/TMI.2016.2538465>.
- [6] A. Kotrotsou, P.O. Zinn, R.R. Colen, Radiomics in brain tumors: an emerging technique for characterization of tumor environment, *Magnetic Resonance Imaging Clinics* 24 (4) (2016) 719–729, <https://doi.org/10.1016/j.mric.2016.06.006>.
- [7] S. Bauer, R. Wiest, L.P. Nolte, M. Reyes, A survey of MRI-based medical image analysis for brain tumor studies, *Phys. Med. Biol.* 58 (13) (2013) R97, <https://doi.org/10.1088/0031-9155/58/13/R97>.
- [8] Delattre, J-Y., Bernsen, H. J. J. A., Frenay, M., Tijssen, C. C., and Grisold, W. (2014). Adjuvant Procarbazine, Lomustine, and Vincristine Chemotherapy in Newly Diagnosed Anaplastic Oligodendroglioma : Long-Term Follow-Up of EORTC Brain Tumor Group Study 26951. *J. Clin. Oncol.* 31 (3), 344–350. doi:10.1200/JCO.2012.43.2229.
- [9] Essig, M., Anzalone, N., Combs, S. E., Dörfler, A., Lee, S-K., Picozzi, P., et al. (2012). MR Imaging of Neoplastic Central Nervous System Lesions: Review and Recommendations for Current Practice. *AJNR Am. J. Neuroradiol* 33 (5), 803–817. doi:10.3174/ajnr.a2640.
- [10] Hosny, A., Parmar, C., Quackenbush, J., Schwartz, L. H., and Aerts, H. J. W. L. (2018). Artificial Intelligence in Radiology. *Nat. Rev. Cancer* 18 (8), 500–510. doi:10.1038/s41568-018-0016-5.
- [11] Razzak, M. I., Naz, S., Zaib, A., and Ahmad, Z. (2018). Deep Learning for Medical Image Processing: Overview, Challenges and the Future. *Lecture Notes Comput. Vis. Biomech.* 26, 323–350. doi:10.1007/978-3-319-65981-7_12.
- [12] Tajbakhsh, N., Shin, J. Y., Gurudu, S. R., Hurst, R. T., Kendall, C. B., Gotway, M. B., et al. (2016). “Convolutional Neural Networks for Medical Image Analysis: Full Training or Fine Tuning?” *IEEE Trans. Med. Imaging* 35 (5), 1299–1312. doi:10.1109/tmi.2016.2535302.
- [13] Seere, S.K.H. and Karibasappa, K., 2020. Threshold segmentation and watershed segmentation algorithm for brain tumor detection using support vector machine. *European Journal of Engineering and Technology Research*, 5(4), pp.516-519.
- [14] Arunkumar, N., Mohammed, M.A., Mostafa, S.A., Ibrahim, D.A., Rodrigues, J.J. and de Albuquerque, V.H.C., 2020. Fully automatic model-based segmentation and classification approach for MRI brain tumor using artificial neural networks. *Concurrency and Computation: Practice and Experience*, 32(1), p.e4962.
- [15] Ullah, H., Batool, A. and Gilanie, G., 2018. Classification of Brain Tumor with Statistical Analysis of Texture Parameter Using a Data Mining Technique. *International Journal of Industrial Biotechnology and Biomaterials*, 4(2), pp.22-36.
- [16] AminKabir Anaraki, MoosaAyati, FoadKazemi, “Magnetic resonance imaging-based brain tumor grades classification and grading via convolutional neural networks and genetic algorithms”, *Biocybernetics and Biomedical Engineering, ELSEVIER*, vol. 39, Issue. 1, , pp. 63–74, January-March 2019.
- [17] Biswas, A. and Islam, M.S., 2021, January. Brain tumor types classification using K-means clustering and ANN approach. In 2021 2nd International Conference on Robotics, Electrical and Signal Processing Techniques (ICREST) (pp. 654-658). IEEE.
- [18] Salçin, K., 2019. Detection and classification of brain tumours from MRI images using faster R-CNN. *Tehnički glasnik*, 13(4), pp.337-342.
- [19] Nandpuru, H.B., Salankar, S.S. and Bora, V.R., 2014, March. MRI brain cancer classification using support vector machine. In 2014 IEEE Students' Conference on Electrical, Electronics and Computer Science (pp. 1-6). IEEE.
- [20] Precious, J., Kirubha, S.P. and Evangeline, I.K., 2022. Automatic Brain Tumor Classification in 2D MRI Images Using Integrated Deep Learning and Supervised Machine Learning Techniques. In *Intelligent Vision in Healthcare* (pp. 131-144). Springer, Singapore.
- [21] Papageorgiou, E.I., Spyridonos, P.P., Glotsos, D.T., Stylios, C.D., Ravazoula, P., Nikiforidis, G.N. and Groumpos, P.P., 2008. Brain tumor characterization using the soft computing technique of fuzzy cognitive maps. *Applied soft computing*, 8(1), pp.820-828.
- [22] Schmeelk, J., 2002. Wavelet transforms on two-dimensional images. *Mathematical and computer modelling*, 36(7-8), pp.939-948.
- [23] Abbas, A.H.; Kareem, A.A.; Kamil, M.Y. Breast Cancer Image Segmentation Using Morphological Operations. *Int. J. Electron. Commun. Eng. Technol.* 2015, 6, 8–14.
- [24] Wang, X.; Liang, G.; Zhang, Y.; Blanton, H.; Bessinger, Z.; Jacobs, N. Inconsistent Performance of Deep Learning Models on Mammogram Classification. *J. Am. Coll. Radiol.* 2020, 17, 796–803.
- [25] Zheng, Y. Breast Cancer Detection with Gabor Features from Digital Mammograms. *Algorithms* 2010, 3, 44–62.
- [26] Van Droogenbroeck, M.; Buckley, M.J. Morphological Erosions and Openings: Fast Algorithms Based on Anchors. *J. Math. Imaging Vis.* 2005, 22, 121–142.
- [27] Beeravolu, A.R.; Azam, S.; Jonkman, M.; Shanmugam, B.; Kannoorpatti, K.; Anwar, A. Preprocessing of Breast Cancer Images to Create Datasets for Deep-CNN. *IEEE Access* 2021, 9, 33438–33463.
- [28] Wang, P.; Wang, J.; Li, Y.; Li, P.; Li, L.; Jiang, M. Automatic classification of breast cancer histopathological images based on deep feature fusion and enhanced routing. *Biomed. Signal. Process. Control* 2021, 65, 102341.
- [29] Simonyan, K.; Zisserman, A. Very deep convolutional networks for large-scale image recognition. *arXiv* 2014, arXiv:1409.1556.
- [30] Shuyue, G.; Murray, L. Breast cancer detection using transfer learning in convolutional neural networks. In *Proceedings of the 2017 IEEE Applied Imagery Pattern Recognition Workshop (AIPR)*, Washington, DC, USA, 10–12 October 2017; pp. 1–8.
- [31] Shallu; Mehra, R. Breast cancer histology images classification: Training from scratch or transfer learning? *ICT Express* 2018, 4, 247–254.
- [32] Hameed, Z.; Zahia, S.; Garcia-Zapirain, B.; Javier Aguirre, J.; María Vanegas, A. Breast Cancer Histopathology Image Classification Using an Ensemble of Deep Learning Models. *Sensors* 2020, 20, 4373.
- [33] Lorencin, I.; Šegota, S.B.; Andelić, N.; Mrzljak, V.; Cabov, T.; Španjol, J.; Car, Z. On Urinary Bladder Cancer Diagnosis: Utilization of Deep Convolutional Generative Adversarial Networks for Data Augmentation. *Biology* 2021, 10, 175.